Progress In Electromagnetics Research M, Vol. 25, 71–85, 2012

COMPLEX RELUCTANCE OF INHOMOGENEOUS EULER-CAUCHY TUBULAR FERRITES TAKING INTO ACCOUNT FREQUENCY-DEPENDENT COMPLEX PERMEABILITY

J. A. Brandão Faria*

Instituto de Telecomunicações, Instituto Superior Técnico, Technical University of Lisbon, Av. Rovisco Pais, Lisboa 1049-001, Portugal

Abstract—This paper presents a novel contribution to the analysis of skin-effect like phenomena in radially inhomogeneous tubular geometries that fit in the category of Euler-Cauchy structures (ECS). The advantage of ECSs is that solutions for the electromagnetic field can be described by very simple closed form formulae. This work addresses the evaluation of the per unit length complex magnetic reluctance of tubular ferrites, taking into account that their complex permeability strongly depends on the frequency. The motivation for this research is linked up with the nascent theory of magnetic transmission lines (MGTL), where the wave guiding structure is made of a pair of parallel ferrimagnetic pieces, and whose performance is critically dependent on the complex magnetic reluctance of its component pieces. The analysis presented is mainly focused on high frequency regimes up into the GHz range.

1. INTRODUCTION

Signal propagation along an electric transmission line (ELTL) is achieved by employing a pair of parallel conductors of high conductivity, immersed in a nonmagnetic insulating dielectric medium. In an ideal ELTL, with perfect conductors ($\sigma \to \infty$), the frequency-domain ($e^{j\omega t}$) transmission line equations read as [1, 2],

$$\begin{cases} \dfrac{d\bar{V}}{dz} = -j\omega L\bar{I} \\ \dfrac{d\bar{I}}{dz} = -j\omega C\bar{V} \end{cases} \tag{1a}$$

Received 22 May 2012, Accepted 21 June 2012, Scheduled 25 June 2012

* Corresponding author: Jose Antonio Marinho Brandão Faria (brandao.faria@ieee.org).

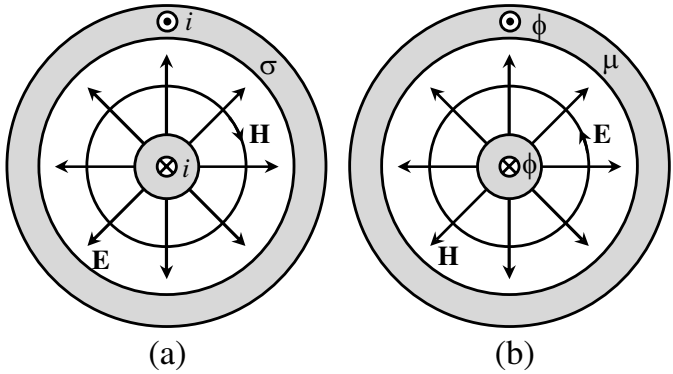

Figure 1. Cross-sectional view of the coaxial cable geometry and associated transverse electromagnetic field. (a) ELTL. (b) MGTL.

where z is the longitudinal axis along which energy flows; $\bar{V}$ and $\bar{I}$ are the line voltage and current phasors; L and C are the per-unit-length (pul) line inductance and capacitance, respectively.

When conductors imperfection is taken into account, a perturbation term (the per-unit-length skin-effect impedance $\bar{Z}_{\text{skin}}$) must be added to the top equation of (1a)

$$\begin{cases} \dfrac{d\bar{V}}{dz} = -\left(j\omega L + \bar{Z}_{\text{skin}}(\omega)\right)\bar{I} \\ \dfrac{d\bar{I}}{dz} = -j\omega C\bar{V} \end{cases} \tag{1b}$$

Magnetic transmission lines (MGTL) are the dual counterpart of ELTLs, where signal propagation is achieved by employing a pair of parallel magnetic pieces of high permeability, immersed in a nonmagnetic insulating dielectric medium. Fig. 1 exemplifies the idea, considering the example of coaxial cable geometry.

If the reader makes a literature search on MGTLs very scarce information will be gotten: a reference to an old patent dated of 1968 aimed at transient suppression in a 60 Hz transformer [3], and a reference to a very recent pending patent claiming its application in terahertz integrated circuits [4]. The concept, the underlying theory, the fabrication, the technology, and the applications of MGTLs are unchartered territory. At this stage, the impact of MGTLs in electrical engineering is speculative, future will tell about MGTL developments.

The theoretical fundamentals of MGTLs have been put forward in [5].

In an ideal MGTL, with perfect magnetic pieces ($\mu \to \infty$), the

frequency-domain transmission line equations are similar to (1a):

$$\begin{cases} \dfrac{d\bar{U}_m}{dz} = -j\omega L \dfrac{1}{R_{WD}^2}\bar{\varphi} \\ \dfrac{d\bar{\varphi}}{dz} = -j\omega C R_{WD}^2\, \bar{U}_m \end{cases} \tag{2a}$$

where, for the same geometrical configuration, C and L are computed as they are for inclusion in (1a); $R_{WD} = \sqrt{\mu_0/\varepsilon_D}$ is the characteristic wave resistance of the dielectric medium; $\bar{U}_m$ is the transverse magnetic voltage between magnetic pieces; $\bar{\varphi} = j\omega\bar{\phi}$, where $\bar{\phi}$ is the phasor representation of the magnetic flux carried by the MGTL pieces.

When magnetic pieces imperfection is taken into account, a perturbation term (the pul complex magnetic reluctance $\bar{R}_m$) must be included in the top equation of (2a)

$$\begin{cases} \dfrac{d\bar{U}_m}{dz} = -\left(j\omega L \dfrac{1}{R_{WD}^2} + \dfrac{\bar{R}_m(\omega)}{j\omega}\right)\bar{\varphi} \\ \dfrac{d\bar{\varphi}}{dz} = -j\omega C R_{WD}^2\, \bar{U}_m \end{cases} \tag{2b}$$

For high frequency regimes, the term $\bar{Z}_{\text{skin}}(\omega)$ in (1b) increases with $\omega^{1/2}$ [1]. Therefore, from (2b), we can see that MGTLs can possibly outperform ELTLs at high frequencies if the term $\bar{R}_m(\omega)$ varies with ω^n, with $n < 3/2$. If $n < 1$ one will have $\bar{R}_m/\omega \to 0$ for increasing frequencies. In conclusion: the calculation of the pul complex reluctance of magnetic pieces is a critical topic for MGTL analysis.

In this paper, we pay attention to a radially inhomogeneous tubular ferrite piece and proceed to the evaluation of its pul complex reluctance as a function of the frequency.

Soft ferrites are ferrimagnetic media oxides of iron combined with divalent transition metals like manganese, nickel, cobalt, magnesium, or zinc. The addition of such metals in various proportions and combinations allows the creation of many different materials whose properties can be tailored for a variety of uses. Ferrites are very poorly conductive materials, and, as such, they combine the properties of a magnetic material with that of an electric insulator [6]. Ferrite losses result from several mechanisms: conduction losses, polarization losses, and magnetization losses. For time harmonic regimes, losses can be taken into account via the imaginary part of the complex permittivity and complex permeability, that is:

$$\bar{\varepsilon} = \varepsilon_0\left(\varepsilon' - j(\varepsilon'' + \sigma/\omega)\right), \quad \bar{\mu} = \mu_0\left(\mu' - j\mu''\right) \tag{3}$$

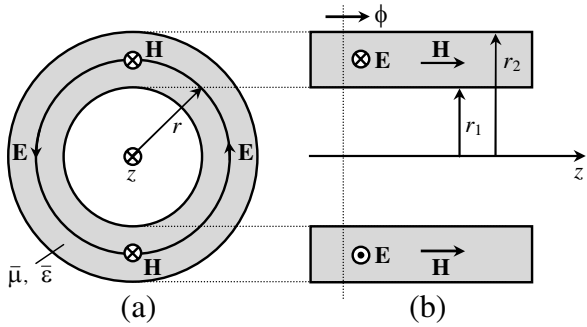

Figure 2. Tubular ferrite. (a) Transversal section. (b) Longitudinal section.

In this paper, the radial dependence of $\bar{\varepsilon}(r)$ and $\bar{\mu}(r)$ is such that the material behaves as an Euler-Cauchy medium [7]. The advantage of this type of medium is that the solution for the electric and magnetic fields can expressed exactly in closed form involving a mere sum of two powers of the radial distance.

Figure 2 depicts transversal and longitudinal sections of the tubular ferrite to be analyzed.

2. ELECTROMAGNETIC FIELD EQUATIONS

2.1. Euler-Cauchy Tubular Conductor

In a recent paper [7], an Euler-Cauchy radially inhomogeneous tubular conductor was analyzed in the frequency domain. Considering the case of very good conductors the Maxwell curl equations

$$\nabla \times \bar{\mathbf{H}} = \sigma \bar{\mathrm{E}} \tag{4}$$

$$\nabla \times \bar{\mathbf{E}} = -j\omega\mu \bar{\mathbf{H}} \tag{5}$$

were utilized to obtain the non-ordinary differential equation governing the axial electric field

$$r^2 \frac{d^2\bar{E}}{dr^2} + r\frac{d\bar{E}}{dr}\left(1 - \frac{r}{\mu}\frac{d\mu}{dr}\right) + \left(r\,\bar{k}(r)\right)^2 \bar{E} = 0 \tag{6}$$

where

$$\bar{k}(r) = \sqrt{-j\omega\mu(r)\sigma(r)} \tag{7}$$

By enforcing the following radial variations for $\mu(r)$ and $\sigma(r)$ in the range $r_1 \leq r \leq r_2$

$$\mu(r) = \mu_2 \left(\frac{r}{r_2}\right)^p, \quad \sigma(r) = \sigma_2 \left(\frac{r_2}{r}\right)^{2+p} \tag{8}$$

it was shown that (6) could be transformed into a homogeneous second order Euler-Cauchy equidimensional equation [8]:

$$r^2\frac{d^2\bar{E}}{dr^2}+\alpha r\frac{d\bar{E}}{dr}+\beta^2\bar{E}=0 \tag{9}$$

where

$$\alpha=1-p=1-\frac{r}{\mu(r)}\frac{d\mu(r)}{dr}=\text{constant independent of } \ r \tag{10}$$

$$\beta^2=-j\omega r^2\mu(r)\sigma(r)=\left(\bar{k}_2r_2\right)^2=\left(\bar{k}_1r_1\right)^2=\text{constant independent of } r \tag{11}$$

where $\bar{k}_1=\bar{k}(r_1)$ and $\bar{k}_2=\bar{k}(r_2)$. The great advantage of (9) is that it has an exact closed form solution, given by the sum of two terms which are powers of the radial coordinate r

$$\bar{E}(r)=E_1\ r^{m_1}+E_2\ r^{m_2} \tag{12}$$

where E_1 and E_2 were obtained from boundary conditions, and where m_1 and m_2 are such that

$$\begin{cases} m_{1,\,2}=p/2\pm\sqrt{(p/2)^2-\beta^2} \\ m_1+m_2=p=1-\alpha \\ m_1m_2=\beta^2=\left(\bar{k}_2r_2\right)^2=\left(\bar{k}_1r_1\right)^2 \end{cases} \tag{13}$$

The pul impedance $\bar{Z}(\omega)$ of the Euler-Cauchy tubular conductor was obtained dividing $\bar{E}(r_2)$ by the current intensity $\bar{I}$ flowing in the conductor, yielding

$$\bar{Z}(\omega)=\frac{\bar{E}(r_2)}{\bar{I}}=\frac{m_2Q^{m_1}-m_1Q^{m_2}}{2\pi r_2^2\sigma_2\left(Q^{m_2}-Q^{m_1}\right)} \tag{14}$$

where Q is the radii ratio of the tubular conductor, $Q=r_2/r_1$.

2.2. Euler-Cauchy Tubular Ferrite

In this work we consider that the tubular ferrite (see Fig. 2) carries a weak magnetic flux $\bar{\phi}$, so that a linear behavior can be assumed.

In the analysis of tubular ferrites (hollow rods), the equations in (4) and (5) must change to

$$\nabla\times\bar{\mathbf{H}}\ =\ j\omega\bar{\varepsilon}\bar{\mathrm{E}} \tag{15}$$

$$\nabla\times\bar{\mathbf{E}}\ =\ -j\omega\bar{\mu}\bar{\mathbf{H}} \tag{16}$$

where the electric field is azimuthal, $\bar{\mathbf{E}}=-\bar{E}\ \hat{\theta}$, and the magnetic field is axial, $\bar{\mathbf{H}}=\bar{H}\ \hat{z}$.

Let us consider a inhomogeneous tubular ferrite where permeability and permittivity are allowed to vary with the radial coordinate, $\bar{\mu}(r)$, $\bar{\varepsilon}(r)$.

The non-ordinary differential equation governing the axial magnetic field is obtained from (15) and (16), yielding

$$r^2 \frac{d^2\bar{H}}{dr^2} + r\frac{d\bar{H}}{dr}\left(1 - \frac{r}{\bar{\varepsilon}}\frac{d\bar{\varepsilon}}{dr}\right) + \left(r\,\bar{k}(r)\right)^2 \bar{H} = 0 \tag{17}$$

where

$$\bar{k}(r) = \omega\sqrt{\bar{\mu}(r)\bar{\varepsilon}(r)} \tag{18}$$

In order to transform (17) into an Euler-Cauchy equation, like in (9), we must enforce

$$\bar{\varepsilon}(r) = \bar{\varepsilon}_2 \left(\frac{r}{r_2}\right)^p, \quad \bar{\mu}(r) = \bar{\mu}_2 \left(\frac{r_2}{r}\right)^{2+p} \tag{19}$$

where p, the inhomogeneity parameter,

$$p = \frac{r}{\bar{\varepsilon}}\frac{d\bar{\varepsilon}}{dr} = \text{ constant independent of } r \tag{20}$$

can be arbitrarily chosen.

The exact closed form solution for the axial magnetic field is given as in (12)

$$\bar{H}(r) = H_1\, r^{m_1} + H_2\, r^{m_2} \tag{21}$$

where m_1 and m_2 are given as in (13):

$$\begin{cases} m_{1,2} = p/2 \pm \sqrt{(p/2)^2 - \beta^2} \\ m_1 + m_2 = p = 1 - \alpha \\ m_1 m_2 = \beta^2 = \left(\bar{k}_2 r_2\right)^2 = \left(\bar{k}_1 r_1\right)^2 \end{cases} \tag{22}$$

but, where,

$$\bar{k}_1 = \omega\sqrt{\bar{\mu}_1\bar{\varepsilon}_1}, \quad \text{and} \quad \bar{k}_2 = \omega\sqrt{\bar{\mu}_2\bar{\varepsilon}_2} \tag{23}$$

In the above expressions we have: $\bar{\mu}_1 = \bar{\mu}(r_1)$, $\bar{\mu}_2 = \bar{\mu}(r_2)$, $\bar{\varepsilon}_1 = \bar{\varepsilon}(r_1)$, and $\bar{\varepsilon}_2 = \bar{\varepsilon}(r_2)$.

3. FIELD SOLUTION OF THE EULER-CAUCHY TUBULAR FERRITE

In order to determine the constants H_1 and H_2 in (21) we must first evaluate the azimuthal electric field inside the tubular conductor. From (15)

$$\bar{\mathbf{E}} = -\bar{E}\,\hat{\theta} = \frac{\nabla \times \bar{\mathbf{H}}}{j\omega\bar{\varepsilon}} = -\frac{1}{j\omega\bar{\varepsilon}}\frac{d\bar{H}}{dr}\hat{\theta}$$

and from (21) we find

$$\bar{E}(r) = \frac{1}{j\omega r\bar{\varepsilon}(r)}\left(H_1 m_1 r^{m_1} + H_2 m_2 r^{m_2}\right) \tag{24}$$

Taking into account that the tubular ferrite carries a z-oriented magnetic flux $\bar{\phi}$, and that $\mathbf{B} \approx 0$ for $0 < r < r_1$, the constants H_1 and H_2 can be obtained by application of Faraday's induction law [1], to circumferential paths of radii r_1 and r_2,

$$\begin{cases} \bar{E}(r_1) = 0 \\ 2\pi r_2 \bar{E}(r_2) = j\omega\bar{\phi} \end{cases} \tag{25}$$

Substituting (25) into (24) we find for H_1 and H_2

$$\begin{cases} H_1 = \xi \times \frac{m_2\, r_1^{-m_1}}{Q^{m_2} - Q^{m_1}} \\ H_2 = \xi \times \frac{m_1\, r_1^{-m_2}}{Q^{m_1} - Q^{m_2}} \end{cases} \quad \text{where} \quad \begin{cases} Q = \frac{r_2}{r_1} \\ \xi = \frac{\bar{\phi}}{2\pi r_2^2 \bar{\mu}_2} \end{cases} \tag{26}$$

Plugging (26) into (21) leads to

$$\bar{H}(r) = \frac{\bar{\phi}}{2\pi\bar{\mu}_2 r_2^2\left(Q^{m_2} - Q^{m_1}\right)}\left(m_2\left(\frac{r}{r_1}\right)^{m_1} - m_1\left(\frac{r}{r_1}\right)^{m_2}\right) \tag{27}$$

4. PER UNIT LENGTH COMPLEX MAGNETIC RELUCTANCE

The pul complex reluctance of the tubular ferrite is obtained from the ordinary definition [1],

$$\bar{U}_m = \bar{R}_m\, \bar{\phi} \tag{28}$$

where $\bar{U}_m = \bar{H}(r_2)$ is the pul magnetic voltage along z on the outer surface of the tubular piece. From (27) we find

$$\bar{R}_m(\omega) = \frac{m_2 Q^{m_1} - m_1 Q^{m_2}}{2\pi r_2^2 \bar{\mu}_2\left(Q^{m_2} - Q^{m_1}\right)} \tag{29}$$

The striking similarity between the formula of the complex reluctance in (29) and the formula of the complex impedance in (14) is worth noting; the role played by σ_2 in (14) is played by $\bar{\mu}_2$ in (29). Note, however, that the roots m_1 and m_2 in (14) and (29) are not the same, because of the definition of $\bar{k}$ in (7) and (18).

To gain more physical insight about the meaning of the pul reluctance in (28) we can use the complex Poynting vector and the complex Poynting theorem [1]. The complex Poynting vector is $\bar{\mathbf{S}}(r) = \frac{1}{2}\bar{\mathbf{E}} \times \bar{\mathbf{H}}^* = -\frac{1}{2}\bar{E}(r)\bar{H}^*(r)\,\hat{r}$. The inward flux of the complex Poynting

vector across the lateral surfaces of the tubular ferrite gives the complex power

$$\bar{P} = \int\limits_{S_{lat}} \bar{\mathbf{S}} \cdot \mathbf{n}_i dS = \tfrac{1}{2} \int\limits_{S_r=r_2} \bar{E}(r_2)\bar{H}^*(r_2)dS - \tfrac{1}{2} \int\limits_{S_r=r_1} \bar{E}(r_1)\bar{H}^*(r_1)dS \quad (30)$$

where, from (25), $\bar{E}(r_1) = 0$ and $\bar{E}(r_2) = j\omega\bar{\phi}/(2\pi r_2)$.

Taking into account that $\bar{H}(r_2) = \bar{U}_m = \bar{R}_m\,\bar{\phi}$, and that $S_{r=r_2} = 1 \times 2\pi r_2$, Equation (30) leads to

$$\bar{P} = j\omega \bar{R}_m^*\, \phi_{\text{rms}}^2 \quad (31)$$

Breaking $\bar{R}_m$ into its real and imaginary parts, $\bar{R}_m = \left(\bar{R}_m\right)_R + j\left(\bar{R}_m\right)_I$, and interpreting the complex power via the complex Poynting theorem we find

$$\bar{P} = \omega\left(\bar{R}_m\right)_I \phi_{\text{rms}}^2 + j\omega\left(\bar{R}_m\right)_R \phi_{\text{rms}}^2 = P_{\text{loss}} + j2\omega\left((W_m)_{av} - (W_e)_{av}\right)$$

From where we conclude

$$\begin{cases} (\bar{R}_m)_R = 2\dfrac{(W_m)_{av} - (W_e)_{av}}{\phi_{\text{rms}}^2} \\ (\bar{R}_m)_I = \dfrac{P_{\text{loss}}}{\omega\phi_{\text{rms}}^2} \end{cases} \quad (32)$$

where P_{loss} denotes the time-averaged ferrite power losses.

According to (32), the reluctance imaginary part $\left(\bar{R}_m\right)_I$ is always positive. Conversely, the reluctance real part $\left(\bar{R}_m\right)_R$ can be either positive or negative; positive when $(W_m)_{av} > (W_e)_{av}$, negative when $(W_e)_{av} > (W_m)_{av}$.

4.1. Low-frequency Approximation

From (22), considering the limit case $\omega \to 0$, ($\beta = 0$), we have $m_1 = p$ and $m_2 = 0$. Also, in that case, magnetization losses are absent, $\bar{\mu} = \mu$. Therefore, from (29) we get

$$\left(\bar{R}_m\right)_{\substack{\omega=0 \\ p\neq 0}} = \frac{p}{2\pi r_2^2 \mu_2 \left(Q^p - 1\right)} \quad (33)$$

The particular situation $p = 0$ leads to an indetermination, which is easily solved by taking into account that

$$\lim_{p\to 0} Q^p \to 1 + p\ln Q$$

from where we find

$$\left(\bar{R}_m\right)_{\substack{\omega=0 \\ p=0}} = \frac{1}{2\pi r_2^2 \mu_2 \ln(Q)} \quad (34)$$

4.2. High-frequency Approximation and Case $p = 0$

The case $p = 0$ and the high-frequency situations are described by the same condition: $\beta \gg p$. From (22), it results $m_1 \approx j\beta$ and $m_2 \approx -j\beta$. Therefore, from (29) we get

$$\left(\bar{R}_m\right)_{HF} = \frac{j\omega}{2\pi r_2}\sqrt{\frac{\bar{\varepsilon}_2}{\bar{\mu}_2}}\left(\frac{Q^{j\beta}+Q^{-j\beta}}{Q^{j\beta}-Q^{-j\beta}}\right) \tag{35a}$$

where, we recall that β is a dimensionless complex given by $\beta = \omega r_2\sqrt{\bar{\mu}_2\bar{\varepsilon}_2}$, and and $Q = r_2/r_1$. Equation (35a) can be given a different look by defining the radii ratio as $Q = e^q$, where

$$q = \ln(r_2/r_1)$$

Substituting $Q = e^q$ into (35a) one obtains

$$\left(\bar{R}_m\right)_{HF} = \frac{\omega}{2\pi r_2 \tan(q\beta)}\sqrt{\frac{\bar{\varepsilon}_2}{\bar{\mu}_2}} \tag{35b}$$

which allow us to foresee that resonance phenomena are certain to occur at periodically spaced frequencies (whenever the time-averaged electric and magnetic energies stored in the tubular ferrite became equal). Resonance peaks do not go to infinity because of the presence of ferrite losses.

4.3. Results Validation

Euler-Cauchy tubular ferrites are not a familiar topic to the literature. Comparison of our results with results already published by other authors is not viable. One simple thing that we can do is to compare the results developed in this paper with already known theoretical results — which is easy for stationary regimes ($\omega = 0$).

For stationary regimes, the azimuthal electric induction field $\mathbf{E}$ originated by $d\phi/dt$ vanishes. Therefore, from (15), the axial magnetic field must obey $\nabla \times \mathbf{H} = 0$, which implies that $H = H_z$ cannot vary with r. Thus we write $H(r) = H_2 =$ constant. However, the magnetic induction field may vary with r because $B(r) = \mu(r)H_2$.

If we take the inhomogeneity parameter $p = -2$, we conclude from (19) that $\mu(r)$ is also r-invariant, $\mu(r) = \mu_2$, and, consequently the magnetic induction field is uniformly distributed in the cross-section of the tubular ferrite, $B(r) = B = \mu_2 H_2$. In this case, the magnetic flux carried by the ferrite piece is $\phi = BS = \mu_2 H_2 \times \pi(r_2^2 - r_1^2)$.

Hence, the magnetic reluctance is

$$R_m = \frac{H_2}{\phi} = \frac{1}{\mu_2 S} = \frac{1}{\mu_2\,\pi(r_2^2 - r_1^2)} \tag{36}$$

Now, if we go back to (29) and make $p = -2$, we find

$$\left(\bar{R}_m\right)_{\substack{\omega=0\\ p\neq 0}} = \frac{-2}{2\pi r_2^2 \mu_2 \left(Q^{-2}-1\right)} = \frac{1}{\mu_2\, \pi (r_2^2 - r_1^2)}$$

which exactly confirms the result in (36).

Another stationary field case that can be validated corresponds to $p = 0$. According to (19), the magnetic permeability depends on r through $\mu(r) = \mu_2 \left(r_2/r\right)^2$. The magnetic induction field is not uniformly distributed in the cross section of the piece: $B(r) = \mu_2 H_2 \left(r_2/r\right)^2$. The magnetic flux is evaluated via

$$\phi = \int\limits_S B(r)\, dS = \int\limits_{r_1}^{r_2} \mu_2 H_2 \left(\frac{r_2}{r}\right)^2 2\pi r dr = 2\pi \mu_2 H_2 r_2^2 \ln\left(\frac{r_2}{r_1}\right)$$

and the corresponding magnetic reluctance is

$$R_m = \frac{H_2}{\phi} = \frac{1}{2\pi r_2^2 \mu_2 \ln\left(r_2/r_1\right)} \tag{37}$$

Now, if we go back to (34), we find, for $p = 0$

$$\left(\bar{R}_m\right)_{\substack{\omega=0\\ p\neq 0}} = \frac{1}{2\pi r_2^2 \mu_2 \ln\left(Q\right)}, \quad \text{with } Q = r_2/r_1$$

which clearly agrees with (37).

In Section 5, dedicated to numerical computations, results will also be validated by resorting to the software code MLCS (Multi-Layered Cylindrical Structures) that was developed in [9] for impedance calculations, and that has suffered minor modifications in order to permit reluctance calculations.

5. NUMERICAL RESULTS AND DISCUSSION

As referred to in Section 1, our focus of attention is on high frequency regimes where MGTLs may possibly find future application. Therefore, as far as simulation results are concerned, attention is only paid to the results developed in Subsection 4.2. In other words, only the case $p = 0$ is addressed.

In this numerical application the following simplifying assumptions are considered. As a poorly conductive material, the ferrite conductivity is neglected. The complex permittivity is assumed to negligibly depend on the frequency, polarization losses being neglected.

On the contrary, the complex magnetic permeability is considered to depend strongly on the frequency, magnetization losses being accounted.

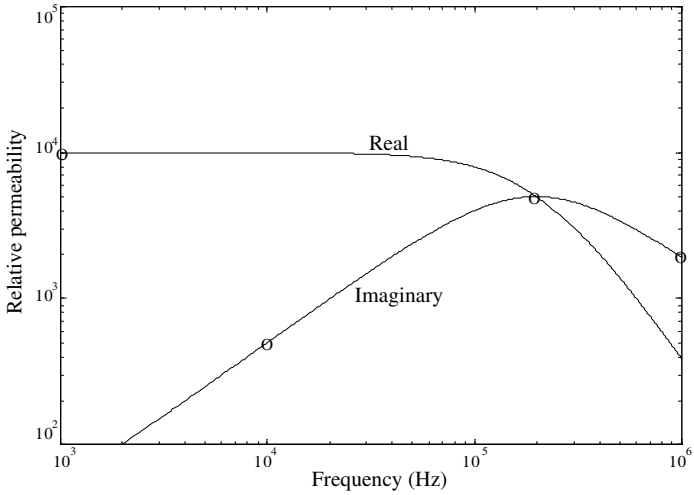

Figure 3. Real and imaginary parts of the relative permeability against frequency. The solid lines describe the complex function in (38). Circle marks correspond to fitting points extracted from Ref. [10].

A MnZn ferrite medium, characterized in a commercial data sheet [10], is employed for exemplification purposes. In [10], a logarithmic plot of the real and imaginary parts of the relative complex permeability is offered in the range 1 kHz to 1 MHz.

Figure 3 depicts a graphical attempt to reproduce the curves shown in [10] capturing their most important features, namely:

Maximum relative permeability: $(\mu_r)_{\max} = (\mu_r)_{\omega=0} = 10^4$.

Real and imaginary parts of the relative permeability equal to $\frac{1}{2}(\mu_r)_{\max}$ at $f = f_0 = 0.2\,\text{MHz}$.

Imaginary part of the relative permeability equal to $\frac{5}{100}(\mu_r)_{\max}$ at $f = 10\,\text{kHz}$, and equal to $\frac{1}{5}(\mu_r)_{\max}$ at $f = 1\,\text{MHz}$.

The curves in Fig. 3 were obtained using the following fitting function

$$\frac{\bar{\mu}_f(f)}{\mu_0} = \underbrace{\left((\mu_r)_\infty + \frac{(\mu_r)_{\max}}{1+(f/f_0)^2}\right)}_{\mu'} - j\underbrace{\left(\frac{(\mu_r)_{\max}}{1+(f/f_0)^2}\left(\frac{f}{f_0}\right)\right)}_{\mu''} \tag{38}$$

where $(\mu_r)_\infty \ll (\mu_r)_{\max}$. We will assume that $(\mu_r)_\infty = 1$.

The following parameters, $r_2 = 5\,\text{mm}$ and $Q = \sqrt{2}$, are assigned to the tubular geometry.

For the case $p = 0$, according to (19), we must have

$$\bar{\varepsilon}(r) = \varepsilon_2 = \varepsilon = \text{constant}, \quad \bar{\mu}(r) = \bar{\mu}_2 \left(\frac{r_2}{r}\right)^2$$

For simulation purposes we considered $\varepsilon = 10\varepsilon_0$ and, from (38),

$$\bar{\mu}_2 = \bar{\mu}(r_2) = \mu_0 + \mu_0 \left(\frac{\frac{1}{2}(\mu_r)_{\max}}{1 + (f/f_0)^2}\right)\left(1 - j\frac{f}{f_0}\right) \tag{39}$$

$$\bar{\mu}_1 = \bar{\mu}(r_1) = Q^2 \bar{\mu}(r_2) = 2\bar{\mu}_2$$

To start with, we evaluated from (34) the tubular ferrite pul reluctance at $f = 0$, yielding

$$(R_m)_{\omega=0} = 2.924 \times 10^6 \ \mathrm{H^{-1}m^{-1}}$$

Next, from (35), we computed the normalized reluctance

$$\left(\bar{R}_m(f)\right)_N = \frac{\left(\bar{R}_m\right)_{HF}}{\left(\bar{R}_m\right)_{\omega=0}} \tag{40}$$

in the range 1 Hz to 1 MHz. Results obtained for the real an imaginary parts of $\left(\bar{R}_m\right)_N$ are shown in Fig. 4. From where we see that the real part remains practically invariant, while the imaginary part starts from zero and increases linearly with f. Note, in addition, that the crossing of the two curves occurs at $f = f_0 = 0.2$ MHz, i.e., when $\mu' = \mu''$.

In order to interpret and discuss the results obtained one should bear in mind that, in the range 1 Hz to 1 MHz, the β factor in (35) is quite small, $\beta = \omega r_2 \sqrt{\bar{\mu}_2 \varepsilon} \ll 1$, and in that case $\tan(q\beta) \approx q\beta$. Therefore, from (35b) and (39) it results

$$\left(\bar{R}_m\right)_{HF} \approx \frac{1}{2\pi r_2^2 \ln(Q)\, \bar{\mu}_2} \approx \frac{1 + j\,(f/f_0)}{2\pi r_2^2 \ln(Q)\, (\mu_2)_{\omega=0}} \tag{41a}$$

It is worth mentioning that the result in (41a) is totally independent of the conductive and dielectric properties of the ferrite. Even if a complex permittivity $\bar{\varepsilon} = \varepsilon_0 (\varepsilon' - j(\varepsilon'' + \sigma/\omega))$ had been enforced, it would play no role at all, insofar $\beta \ll 1$.

By using (41a), the normalized reluctance is obtained

$$\left(\bar{R}_m\right)_N \approx 1 + j\,(f/f_0) \tag{41b}$$

which clearly justifies the computation results offered in Fig. 4.

We run MLCS for $f = 1$ Hz, 1 kHz, and 1 MHz. The circle marks superposed to the solid lines in Fig. 4 correspond to output results from MLCS. The agreement is remarkable.

Let us now explore the frequency window from 20 MHz to 20 GHz, where $f \gg f_0$. The computation of the normalized reluctance in (40)

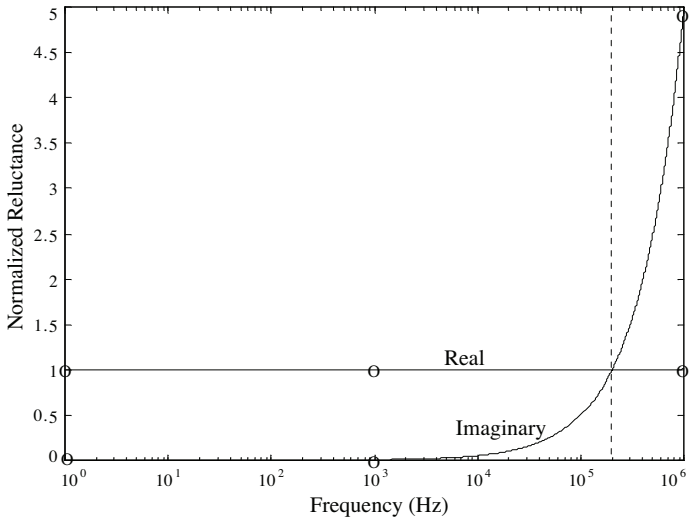

Figure 4. Real and imaginary parts of the normalized complex reluctance against frequency in the range 1 Hz to 1 MHz. Solid lines were obtained from (40), (35) and (39). Circle marks were obtained using MLCS algorithm [9].

produces the graphic plot shown in Fig. 5, with huge values for both the real and imaginary parts, with the real part changing from positive to negative values. We are observing the first resonance phenomenon we alluded to at the end of Subsection 4.2.

For $f \gg f_0$ the complex permeability $\bar{\mu}_2$ in (39) simplifies to

$$\bar{\mu}_2 \approx \mu_0 \left(1 - j\kappa/2\right), \quad \kappa = (\mu_r)_{\max} f_0/f \tag{42}$$

where κ is about 10^{-1} at 10 GHz. Consequently, $\left(\bar{R}_m\right)_{HF}$ in (35) transforms into

$$\left(\bar{R}_m\right)_{HF} \approx \frac{\omega(1 + j\kappa/2)}{2\pi r_2 \tan(\vartheta(1 - j\kappa/2))} \sqrt{\frac{\varepsilon}{\mu_0}} \ , \quad \vartheta = q r_2 \omega \sqrt{\varepsilon\mu_0} \tag{43}$$

The first resonance event occurs when the tangent function in the denominator approaches zero, that is, when $\vartheta \approx \pi/2$. The corresponding resonance frequency is

$$f_r = \frac{1}{4 q r_2 \sqrt{\varepsilon\mu_0}} \approx 15\,\text{GHz}$$

which is confirmed in Fig. 5.

Note that, contrary to the case $\beta \ll 1$, here, the behavior of the complex reluctance does depend on the ferrite dielectric properties.

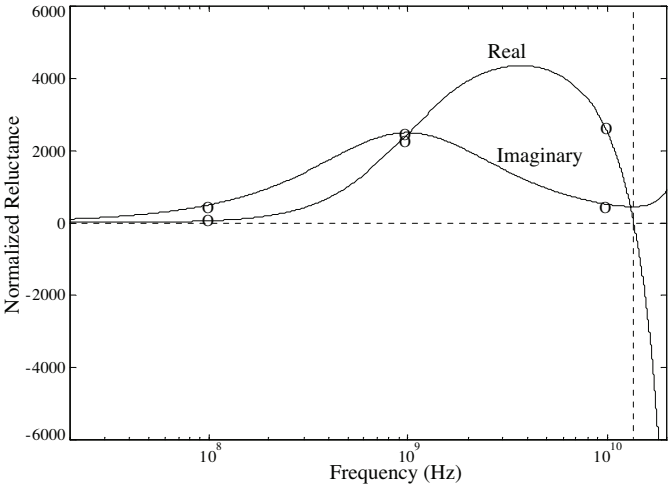

Figure 5. Real and imaginary parts of the normalized complex reluctance against frequency in the range 20 MHz to 20 GHz. Solid lines were obtained from (40), (35) and (39). Circle marks were obtained using MLCS algorithm [9].

For validation purposes we rerun MLCS for $f = 0.1$ GHz, 1 GHz, and 10 GHz. The circle marks superposed to the solid lines in Fig. 5 correspond to output results from MLCS. Again, the agreement is quite good.

6. CONCLUSION

Magnetic transmission lines (MGTL) are an open field of research; they can guide an electromagnetic wave by using a pair of parallel ferrimagnetic pieces carrying a magnetic flux. Preliminary studies on MGTLs have raised the possibility that MGTLs can perform better than ordinary electric transmission lines at very high frequencies. However, such a possibility is critically dependent on the longitudinal magnetic voltage drop along the two pieces, that is to say that MGTL performance requires a detailed knowledge of the per unit length complex reluctance of its component pieces.

This paper addressed the theoretical analysis, and the computation, of the per unit length complex reluctance of an inhomogeneous Euler-Cauchy tubular ferrite, where the frequency-dependent features of the complex magnetic permeability are taken into account. Computation results covering the range 1 Hz to 20 GHz were obtained and

validated. For frequencies up to 1 MHz the real part of the complex reluctance remains practically independent of the frequency, whereas the imaginary part increases linearly. However, in the gigahertz band, a remarkable resonance effect, with very large values of the complex reluctance, showed up.

Results obtained were based on data pertaining to a particular ferrite specimen, and cannot be generalized; in fact, ferrite behavior is strongly dependent on its chemical composition, which may vary a lot among specimens.

ACKNOWLEDGMENT

FCT — the Portuguese Foundation for Science and Technology sponsored this work (Project PTDC/EEI-TEL/1448/2012).

REFERENCES

1. Faria, J., *Electromagnetic Foundations of Electrical Engineering*, Wiley, Chichester, 2008.
2. Magnusson, P., G. Alexander, V. Tripathi, and A. Weisshaar, *Transmission Lines and Wave Propagation*, 4th Edition, CRC Press, Boca Raton, 2001.
3. Kerns, Q. A., "Transient-suppressing magnetic transmission line," Patent US 3376523, Apr. 2, 1968.
4. Faria, J., "Dispositivo formado por uma linha magnética de transmissão para uso em circuitos integrados para aplicações na tecnologia Terahertz, (Magnetic transmission line device for terahertz integrated circuits)," Patent PT 106056, Dec. 12, 2011.
5. Faria, J. and M. P. Pires, "Theory of magnetic transmission lines," *IEEE Trans. Microw. Theory Tech.*, Paper TMTT-2012-05-0407.
6. Horvath, M. P., "Microwave applications of soft ferrites," *J. Magnetism Magn. Mat.*, Vols. 215–216, 171–183, 2000.
7. Faria, J., "Skin effect in inhomogeneous Euler-Cauchy tubular conductors," *Progress In Electromagnetics Research M*, Vol. 18, 89–101, 2011.
8. Wylie, C., *Advanced Engineering Mathematics*, McGraw-Hill, New York, 1975.
9. Faria, J., "A matrix approach for the evaluation of the internal impedance of multilayered cylindrical structures," *Progress In Electromagnetics Research B*, Vol. 28, 351–367, 2011.
10. http://www.fair-rite.com/newfair/materials76.htm.